2016

Soluble Amyloid-β42 Stimulates Glutamate Release through Activation of the α7 Nicotinic Acetylcholine Receptor.

Kevin N Hascup

Erin R Hascup

Recommended Citation

Hascup, Kevin N and Hascup, Erin R. "Soluble Amyloid-β42 Stimulates Glutamate Release through Activation of the α7 Nicotinic Acetylcholine Receptor.." *Journal of Alzheimer's disease : JAD* (Jan 2016). doi:10.3233/JAD-160041.

Soluble Amyloid-β42 Stimulates Glutamate Release through Activation of the α7 Nicotinic Acetylcholine Receptor

Kevin N. Hascup[1] & *Erin R. Hascup[1,2]*

[1]Department of Neurology, Center for Alzheimer's Disease and Related Disorders, Neurosciences Institute, Center for Integrated Research in Cognitive & Neural Sciences, [2]Department of Pharmacology, Southern Illinois University School of Medicine, Springfield, IL, USA

Running Title: Aβ42 Evokes Glutamate Release by α7nAChR

*Corresponding author: Hascup, ER, Department of Neurology, Center for Alzheimer's Disease and Related Disorders, Southern Illinois University School of Medicine, P.O. Box 19628, Springfield, IL 62794-9628, USA, Tel: 217-545-6988; Email: ehascup@siumed.edu

Abbreviations: 1,3 Phenylenediamine dihydrochloride (mPD); alpha 7 nicotinic acetylcholine receptor (α7nAChR); alpha bungarotoxin (aBTx); Alzheimer's disease (AD); amyloid beta (Aβ); analysis of variance (ANOVA); L-ascorbic acid (AA); bovine serum albumin (BSA); dentate gyrus (DG); dopamine hydrochloride (DA); Fast Analytical Sensing Technology (FAST); hydrogen peroxide (H_2O_2); microelectrode array (MEA); phosphate buffered saline (PBS); platinum (Pt); standard error of the mean (SEM); tetrodotoxin (TTX)

Abstract

Alzheimer's disease (AD) is an age-related neurodegenerative disorder characterized by progressive memory loss and hippocampal atrophy. Soluble amyloid-β (Aβ)$_{42}$ and plaque accumulation is implicated as the neurotoxic species in this disorder, however, at physiological concentrations (pM-nM), Aβ$_{42}$ contributes to neurogenesis, long-term potentiation, and neuromodulation. Because Aβ$_{42}$ binds the α7 nicotinic acetylcholine receptors (α7nAChRs) located presynaptically on glutamatergic terminals, involved with hippocampal dependent learning and memory, we examined the effects of the human, monomeric isoform of Aβ$_{42}$ on glutamate release in the dentate gyrus (DG), CA3, and CA1, of isoflurane anesthetized, 6-9 month old male C57BL/6J mice. We utilized an enzyme-based microelectrode array selective for L-glutamate measures with fast temporal (4 Hz), low spatial resolution (50 x 100 µm) and minimal damage to the surrounding parenchyma (50-100 µm). Local application of Aβ$_{42}$ (0.01, 0.1, 1.0, and 10.0 µM; ~150 nl; 1-2 seconds) elicited robust, reproducible glutamate signals in all hippocampal subfields studied. Local application of 0.1 and 1.0 µM Aβ$_{42}$ significantly increased the average maximal amplitude of glutamate release compared to saline in the DG and CA1. 10.0 µM Aβ$_{42}$ significantly elevated glutamate release in the DG and CA3, but not in the CA1. Glutamate release was completely attenuated with coapplication of 10.0 µM α-Bungarotoxin, the potent α7nAChR antagonist. Coapplication of 10.0 µM tetrodotoxin, indicates Aβ$_{42}$ induced glutamate release originates from neuronal rather than glial sources. This study demonstrates that the human, monomeric Aβ$_{42}$ isoform evokes glutamate release through the α7nAChR and varies across hippocampal subfields.

Keywords: Alzheimer's disease, amyloid beta, cognition, biosensor, neurotransmission, presynaptic, tetrodotoxin, alpha bungarotoxin, hippocampus, nicotinic acetylcholine receptor

Introduction

Alzheimer's disease (AD) is an age-related neurodegenerative disorder characterized by progressive memory loss, cognitive decline, and hippocampal atrophy. The hallmark pathological features of AD includes amyloid-β (Aβ) plaques and neurofibrillary tangles with evidence supporting abnormal accumulation of Aβ followed by tau-mediated neuronal injury and dysfunction [1]. This process, referred to as the amyloid cascade hypothesis, proposes that Aβ initiates the series of pathological events leading to neuronal dysfunction, cell death, and the eventual cognitive impairments observed in AD [2]. In AD brains, $A\beta_{40}$ and $A\beta_{42}$ are the predominant peptide isoforms, the latter of which is believed to aggregate faster and thusly considered more neurotoxic [3]. For example, recent evidence supports soluble $A\beta_{42}$ dimers as the neurotoxic isoform precipitating AD pathology [4–6].

However, at physiological concentrations (pM-nM) experimental evidence suggests Aβ has a role in normal brain functions including neurogenesis, long-term potentiation, and neurotransmitter modulation [7–9]. $A\beta_{42}$ binds to the α7 nicotinic acetylcholine receptor (α7nAChR) with picomolar affinity [10] and activation of this receptor is known to stimulate glutamate release [11]. Glutamate, the predominant excitatory neurotransmitter in the mammalian CNS, has a strong prevalence in neocortical and hippocampal pyramidal neurons and, therefore, plays a critical role in learning and memory [12]. Furthermore, picomolar concentrations of $A\beta_{42}$ can enhance synaptic plasticity and reference memory through activation of the α7nAChR [13]. These data suggest that endogenous $A\beta_{42}$ formation lies on a continuum whereby low concentrations of the peptide are important for normal brain function, however, when a concentration threshold is crossed; accumulation and aggregation dominate leading to neurotoxicity [7].

The purpose of the present study was to elucidate whether $A\beta_{42}$ could evoke hippocampal glutamate release through the α7nAChR.

Because of the rapid (msec) clearance of glutamate from the extracellular space by the high-affinity excitatory amino acid transporters [14,15] few studies have been capable of directly measuring glutamatergic neurotransmission on a subsecond timescale. To do this, we utilized an enzyme-based microelectrode array (MEA) coupled with constant potential amperometry to independently measure glutamate release in the dentate gyrus (DG), CA3, and CA1 of isoflurane anesthetized C57BL/6J mice. These MEAs have fast temporal (4 Hz) [16], low spatial (50 x 100 μm) resolution and minimal damage to the surrounding parenchyma (50-100 microns) [17]. A glass micropipette was attached to the MEA to locally apply varying concentrations of $A\beta_{42}$ (0.01 – 10.0 μM). While standard practice is to report the concentration of solutions in the glass micropipette, it should be noted that pressure ejection of solutions from a micropipette *in vivo* act as a point source with the concentration decreasing as the distance increases from the ejection site [18]. We have determined that a tenth of the barrel concentration is diffusing to the MEA surface, which is considered further in the discussion section. The results presented here support the ability of soluble $A\beta_{42}$ to stimulate the α7nAChR leading to glutamate release that varies among hippocampal subfields.

Materials & Methods

Animals: Six to nine month-old, male C57BL/6J mice were obtained from Jackson Laboratory (Bar Harbor, ME). Protocols for animal use were approved by the *Laboratory Animal Care and Use Committee* at Southern Illinois University School of Medicine. Animals were group housed on a 12:12 hour light: dark cycle, and food and water were available *ad libitum*. Immediately following experimentation, mice were euthanized with an overdose of isoflurane and decapitated. Brains were fixed in 4% paraformaldehyde for histological assessment of MEA placement.

Chemicals: All chemicals were prepared and stored according to manufacturer recommendations unless otherwise noted. Human $A\beta_{42}$ was obtained from Anaspec, Inc (Fremont, CA), and stored at -80°C in 0.1 mM aliquots. Alpha-bungarotoxin (αBTx) and tetrodotoxin (TTX) were obtained from Tocris Bioscience (Minneapolis, MN). L-glutamate oxidase (EC 1.4.3.11) was obtained from Cosmo Bio Co. (Carlsbad, CA) and diluted in distilled, deionized water (ddH$_2$O) to make a 1U/µl stock solution for storage at 4°C. Sodium phosphate monobasic monohydrate, sodium phosphate dibasic anhydrous, 1,3 phenylenediamine dihydrochloride (mPD), sodium chloride and hydrogen peroxide (H$_2$O$_2$, 30% in water) were obtained from Thermo Fisher Scientific (Waltham, MA). L-glutamic acid sodium salt, bovine serum albumin (BSA), glutaraldehyde, dopamine hydrochloride (DA) and L-ascorbic acid (AA) were obtained from Sigma-Aldrich Co. (St. Louis, MO).

SDS-PAGE: All chemicals were obtained from Bio-Rad (Hercules, CA). $A\beta_{42}$ samples were prepared similar to *in vivo* experiments to determine peptide isoform. 0.1 mM $A\beta_{42}$ was removed from -80°C and allowed to thaw for 30 min at 4°C. $A\beta_{42}$ was serially diluted in physiological saline (pH 7.4) to the following concentrations 10.0, 1.0, 0.1, 0.01, and 0.001 µM. A 1:4 ratio of tricine sample buffer to

Aβ₄₂ was prepared and loaded into the wells of a 4-20% Tris-HCl gel and run for ~90 min at 120V in 1x Tris-Tricine-SDS buffer. The gel was fixed with 40% methanol / 10% acetic acid for 30 min, rinsed with ddH$_2$O and stained with Coomassie G-250 Stain for 60 min on a rotator. The Coomassie G-250 Stain was rinsed twice with ddH$_2$O in one hour intervals on a rotator and imaged using a Fluor-S® MultiImager (Bio-Rad).

Enzyme-Based Microelectrode Arrays: Enzyme-based MEAs with platinum (Pt) recording surfaces (Figures 1A & B) were fabricated, assembled, coated, and calibrated for *in vivo* mouse glutamate measurements as previously described [19–21]. Briefly, one of the R2 MEA Pt sites was coated with an L-glutamate oxidase, BSA, glutaraldehyde coating solution. BSA and glutaraldehyde increase the adhesion and crosslink L-glutamate oxidase to the MEA surface. L-glutamate oxidase enzymatically degrades glutamate to α-ketoglutarate and the electroactive reporter molecule, H$_2$O$_2$. The second Pt recording site (self-referencing or sentinel site) was coated similar to the glutamate recording site, except L-glutamate oxidase was omitted from the coating solution; therefore, unable to enzymatically generate H$_2$O$_2$ from L-glutamate. A potential of +0.7 V vs a Ag/AgCl reference electrode was applied to the Pt recording surface, resulting in a two electron oxidation of H$_2$O$_2$ and the current was amplified and digitized by the Fast Analytical Sensing Technology (FAST) 16mkIII (Quanteon, LLC; Nicholasville, KY) electrochemistry instrument.

mPD Electropolymerization: A minimum of 72 hrs after enzyme coating, Pt recording surfaces were electroplated with 5 mM mPD in 0.05 M phosphate buffered saline (PBS) [22]. FAST electroplating software applied a triangular wave potential with a -0.5 V offset and 0.25 V peak-to-peak amplitude at 0.05 Hz for 20 min to create an exclusion layer that restricts the passage of AA, DA, uric acid, and 3,4-dihydroxyphenylacetic acid.

Calibration: A minimum of 24 hrs after mPD electropolymerization, each MEA was calibrated prior to implantation to generate a standard curve for the conversion of current to glutamate concentration [23]. The Pt recording sites and a glass Ag/AgCl reference electrode (Bioanalytical Systems, Inc., West Lafayette, IN) were placed in a continuously stirred solution 0.05 M PBS (40.0 mL) maintained at 37°C with a recirculating water bath (Stryker Corp., Kalamazoo, MI). Final beaker concentrations of 250 µM AA, 20, 40, and 60 µM L-glutamate, 2 µM DA, and 8.8 µM H_2O_2 were used to assess MEA performance. After the H_2O_2 addition, a final beaker concentration of 0.25 µM $A\beta_{42}$ was added to test that $A\beta_{42}$ was not inherently electrochemically active (Figure 1C). Forty MEAs (24 unique) were used with an average ± standard error of the mean (SEM) for glutamate sensitivity of 9.2 ± 0.6 pA/µM (r^2 = 0.998 ± 0.001), selectivity ratio of 1031 ± 282 to 1, and limit of detection (LOD) of 0.3 ± 0.1 µM based on a signal-to-noise ratio of 3. All MEAs were selected based upon LOD levels lower than the expected *in vivo* glutamate response.

Microelectrode Array / Micropipette Assembly: A glass micropipette (1.0 mm outer diameter, 0.58 mm internal diameter; World Precision Instruments, Inc., Sarasota, FL) was used to locally apply solutions to the mouse hippocampal subfields. Glass micropipettes were pulled using a vertical micropipette puller (Sutter Instrument Co., Novato, CA) and the tip was "bumped" to create an internal diameter of 12-15 µm. The tip of the micropipette was positioned between the pair of recording sites and mounted 100 µm above the MEA surface. The micropipettes were filled with sterile filtered (0.20 µm) solutions of physiological saline (0.9% NaCl, pH 7.4), 0.01 – 10.0 µM $A\beta_{42}$, 0.1 µM $A\beta_{42}$ with 10.0 µM αBTx or 0.1 µM $A\beta_{42}$ with 10.0 µM TTX all diluted in physiological saline. Fluid was pressure-ejected from the glass micropipette using a Picospritzer III (Parker-Hannafin, Cleveland, OH), with pressure (5-15 psi) adjusted to consistently deliver volumes between 100-200 nl over 1-2 s intervals. Ejection volumes were monitored with a stereomicroscope (Luxo Corp., Elmsford, NY) fitted with a calibrated reticule [24].

Reference Electrode: A Ag/AgCl reference electrode was prepared by stripping 5 mm of Teflon® off each end of a silver wire (200 µm bare, 275 µm coated; A-M Systems, Carlsberg, WA). One end was soldered to a gold-plated test connector (Newark element14 Chicago, IL) and the other was coated with AgCl by placing the tip of the sliver wire (cathode) into a 1 M HCl plating bath saturated with NaCl containing a stainless steel wire (anode) and applying +9 V DC using a power supply to the cathode *vs* the anode for 15 min.

In Vivo Anesthetized Recordings: Mice were anesthetized using 1.5-2.0% isoflurane (Abbott Lab, North Chicago, IL) in a calibrated vaporizer (Vaporizer Sales & Service, Inc., Rockmart, GA) and prepared for *in vivo* electrochemical recordings as described elsewhere [20]. The mouse was placed in a stereotaxic frame (David Kopf Instruments, Tujunga, CA) fitted with a mouse anesthesia mask and body temperature was maintained at 37°C with a water pad connected to a recirculating water bath. A craniotomy was performed to access the hippocampus. The Ag/AgCl reference wire was remotely implanted in the right cortex. Using a microdrive (Narishige International, East Meadow, NY) attached to the electrode holder of the stereotaxic arm, the MEA / micropipette assembly was lowered into the DG (AP: -2.0, ML: ± 1.0, DV: -2.2 mm), CA3 (AP: -2.0, ML: ± 2.0, DV: -2.2 mm) and CA1 (AP: -2.0, ML: ± 1.0, DV: -1.7 mm), from Bregma that was randomly assigned for each mouse [25]. Each hemisphere was randomly assigned to a different treatment group to minimize the number of mice used. Constant voltage amperometry (4 Hz) was performed using the FAST16mkIII and FAST software for multi-channel simultaneous recordings [26]. MEAs were allowed to reach a stable baseline for 60 min before basal glutamate determination and pressure ejection studies.

Data Analysis: The FAST16MkIII electrochemical instrument and FAST software saves amperometric data, time and pressure ejection events for all recording sites. Calibration data, in conjunction with a MATLAB (MathWorks, Natick, MA) graphic user interface program

developed by Jason Burmeister Consulting, LLC (Version 6.1) was used to calculate basal glutamate and $A\beta_{42}$-evoked glutamate release. To determine extracellular glutamate concentration, the sentinel site current (pA) was subtracted from the glutamate recording site current (pA) and divided by the slope (pA/μM) obtained during the calibration [26–29]. Basal glutamate was calculated by taking a 10 s baseline average prior to starting $A\beta_{42}$ pressure ejections in the DG, CA3, and CA1 and both hemispheres were averaged to create a single data point per mouse. Five reproducible signals were evoked in each hippocampal subfield and averaged into a representative signal for comparison between concentrations. Prism (GraphPad Software, Inc., La Jolla, CA) software was used for statistical analyses. A one-way analysis of variance (ANOVA) followed by a Fisher's LSD *post-hoc* test was used to compare concentrations of $A\beta_{42}$ to saline control. An unpaired, two-tailed Student's t-test was used to compare glutamate dynamics from coapplication of both 0.1 μM $A\beta_{42}$ with 10.0 μM aBTx and 0.1 μM $A\beta_{42}$ with 10.0 μM TTX to 0.1 μM $A\beta_{42}$. Outliers were identified with a single Grubbs' test (alpha = 0.05) per group. Data are represented as mean ± SEM and statistical significance was defined as $p<0.05$. Throughout the manuscript, sample size refers to the number of animals in each hippocampal subfield.

Results

We characterized the $A\beta_{42}$ peptide conformation by using gel electrophoresis methods. With SDS-PAGE, the preparations analyzed resolved to a 4.5 kDA species consistent with the monomeric isoform that was visible at the 10.0, 1.0, and 0.1 μM $A\beta_{42}$ concentrations (Figure S1). However, the lowest concentrations of $A\beta_{42}$ (0.01 and 0.001 μM) resulted in undetectable levels.

Basal Glutamate

Prior to local application studies, basal glutamate measures were assessed. Basal glutamate was similar among the DG (1.5 ± 0.3 µM; n=30), CA3 (2.0 ± 0.3 µM; n=31), and CA1 (1.9 ± 0.3 µM; n=29) hippocampal subfields as shown in Figure 2. Sample size refers to the number of animals in each hippocampal subfield.

Local application of Aβ$_{42}$

We locally applied similar volumes (Figure 3A) of 4 different Aβ$_{42}$ concentrations (0.01, 0.1, 1.0, and 10.0 µM; n=9 per dose) and physiological saline (n=8-9) as vehicle control in the DG, CA3, and CA1 hippocampal subfields. Local application of 0.1 µM Aβ$_{42}$ elicited robust, reproducible glutamate signals in the mouse DG (Figure 3B), CA3, and CA1. When the maximal amplitude of Aβ$_{42}$-evoked glutamate release was averaged, (Figure 3C), local application of 0.1 µM (p = 0.0002), 1.0 µM (p = 0.04), and 10.0 µM (p = 0.03) Aβ$_{42}$ elicited significantly more glutamate than saline control (F(4,40) = 5.170; p = 0.002) in the DG. Evoked glutamate release from local application of 0.01 µM Aβ$_{42}$ (p = 0.54) was similar to saline control in the DG. In the CA3, we observed that local application of 1.0 µM (p = 0.04) and 10.0 µM (p = 0.001) Aβ$_{42}$ elicited significantly more glutamate than saline control (F(4,39) = 3.195; p = 0.02). Evoked glutamate release from local application of 0.01 µM (p = 0.17) and 0.1 µM (p = 0.08) Aβ$_{42}$ resulted in evoked glutamate release that was not statistically significant from saline control in the CA3. Evoked glutamate release from local application of 0.01 µM (p = 0.02), 0.1 µM (p = 0.0005), and 1.0 µM (p = 0.009) Aβ$_{42}$ was significantly elevated compared to saline control (F(4,40) = 4.226; p = 0.006) in the CA1. However, evoked glutamate release from local application of 10.0 µM (p = 0.21) Aβ$_{42}$ was statistically similar to saline control in the CA1.

Coapplication of 0.1 µM Aβ$_{42}$ with 10.0 µM αBTx

To determine the contribution of glutamate release through activation of the α7nAChR, the irreversible antagonist, αBTx (10.0 µM) was coapplied with 0.1 µM Aβ$_{42}$. Previous studies have shown that 10.0 µM αBTx attenuates nicotine-induced glutamate release in the prefrontal cortex of awake, freely behaving rats [11]. The concentration of Aβ$_{42}$ peptide was chosen since it elicited the largest glutamate release in both the DG and the CA1 and was not statistically different from the 10.0 µM Aβ$_{42}$ response observed in the CA3. When similar volumes of 0.1 µM Aβ$_{42}$ with 10.0 µM αBTx and 0.1 µM Aβ$_{42}$ alone (Figure 4A) was locally applied in the DG ($F_{(4,8)} = 1.598$; $p = 0.70$), CA3 ($F_{(4,8)} = 2.259$; $p = 0.32$), and CA1 ($F_{(4,8)} = 1.680$; $p = 0.40$) the glutamate response was attenuated in the DG, CA3, and CA1 (Figure 4B), resulting in a similar response to that observed with local application of saline vehicle. When these signals were averaged (Figure 4C), coapplication of 0.1 µM Aβ$_{42}$ with 10.0 µM αBTx significantly attenuated glutamate release compared to local application of 0.1 µM Aβ$_{42}$ in the DG ($F_{(4,8)} = 6.267$; $p = 0.02$), CA3 ($F_{(4,8)} = 9.397$; $p = 0.04$), and CA1 ($F_{(4,8)} = 13.56$; $p = 0.003$).

Coapplication of 0.1 µM Aβ$_{42}$ with 10.0 µM TTX

To determine the neuronal versus glial contribution of Aβ$_{42}$-evoked glutamate release, the reversible sodium channel blocker, TTX (10.0 µM) was coapplied with 0.1 µM Aβ$_{42}$ alone. When similar volumes of 0.1 µM Aβ$_{42}$ with 10.0 µM TTX and 0.1 µM Aβ$_{42}$ (Figure 4A) was locally applied in the DG ($F_{(9,8)} = 1.020$; $p = 0.38$), CA3 ($F_{(9,8)} = 1.895$; $p = 0.75$), and CA1 ($F_{(9,8)} = 1.185$; $p = 0.51$) the glutamate response was no longer present and a decrease in basal glutamate levels was observed in the DG, CA3, and CA1 (Figure 4B). When these signals were averaged (Figure 4C), coapplication of 0.1 µM Aβ$_{42}$ with 10.0 µM αBTx significantly attenuated glutamate release

compared to local application of 0.1 μM Aβ$_{42}$ in the DG ($F_{(9,8)}$ = 1.808; p = 0.001), CA3 ($F_{(9,8)}$ = 1.615; p = 0.003), and CA1 ($F_{(9,8)}$ = 1.004; p < 0.0001).

Discussion

The data presented in this manuscript indicates that local application of monomeric soluble Aβ$_{42}$ evokes glutamate release through the α7nAChR in all three hippocampal subfields studied. Magdesian and colleagues [30] have demonstrated that Aβ binds at the interface between the acetylcholine and nicotine binding domains of the α7nAChR. Additionally, Aβ-evoked Ca^{2+} efflux from nerve terminals was not increased after coapplication of nicotine suggesting similar binding sites [31,32]. Since nicotine has been shown to evoke glutamate release via the α7nAChR [11], these studies support Aβ$_{42}$ binding near the nicotinic site on α7nAChR to evoke glutamate release.

Conflicting data exists in the literature regarding the α7nAChR-Aβ interaction with studies supporting both receptor activation and inhibition [33]. These differences may be related to the model system employed as well as the aggregation state and concentration of Aβ used. We selected the anesthetized mouse as our model system since this provides us with the complete hippocampal afferent / efferent connections as well as contribution from astrocytes (glutamate uptake and/or gliotransmission). Using SDS-PAGE we have confirmed that we are locally applying the monomeric isoform of Aβ$_{42}$. Finally the concentration of Aβ is the largest confounding variable in the literature. Physiological concentrations of Aβ (pM to low nM) have been shown to potentiate neurotransmitter release while supraphysiological concentrations (high nM to μM) inhibit neurotransmitter release [8]. While standard practice is to report the concentration of solutions in the glass micropipette, it should be noted that pressure ejection of solutions from a micropipette *in vivo*

12

act as a point source with the concentration decreasing as the distance increases from the ejection site [18]. Using the effective diffusion coefficient of monomeric $A\beta_{42}$ ($0.623*10^{-6}$ cm^2s^{-1}) as calculated by Waters [34] and the pressure ejection diffusion equation derived from Nicholson [18] we have calculated an approximate concentration of $A\beta_{42}$ surrounding the MEA. Based on an average distance of 100 microns from the micropipette (point source) to the MEA, we have approximated the concentration of locally applied $A\beta_{42}$ surrounding the MEA to be 1.0, 10.0, 100.0 and 1000.0 nM (for micropipette concentration of 0.01, 0.1, 1.0 and 10.0 µM $A\beta_{42}$, respectively) after a 1 second pulse of ~150 nl of solution. While this is a theoretical approximation, these diffusion concentrations are in agreement with the literature, whereby the physiological pM to low nM concentrations evoked the largest glutamate release in the DG and CA1. Coincidentally, in the APP/PS1 mouse model of increased $A\beta_{42}$ production we have noticed that the earliest increases in glutamate release are observed in the CA1 [16] and DG (unpublished observations). These data are consistent with the concept that physiological concentrations of $A\beta$ modulate neurotransmitter release essential for synaptic plasticity and learning and memory [7,13].

The most striking results from this study are the differences in $A\beta_{42}$-evoked glutamate release among the hippocampal subfields. The largest glutamate responses were observed with 0.1 µM $A\beta_{42}$ in the DG and CA1, while 10.0 µM produced a slightly larger glutamate response in the CA3. These discrepancies might be attributable to the distribution of α7nAChR in the rodent hippocampus. Autoradiographic studies indicate αBTx binding sites are slightly weaker in the CA3 compared to the DG and CA1 subfields [35]. Fewer CA3 α7nAChRs may help to explain why the highest concentration of $A\beta_{42}$ tested evoked the largest release of glutamate in this hippocampal subfield. Interestingly, $A\beta$ protein deposition in humans with AD has been shown to occur first in the CA1 and DG followed by the CA3 [36], similar to the pattern we observed with increased $A\beta_{42}$-evoked glutamate release at lower concentrations in the CA1

and DG. Regardless, the demonstration of $A\beta_{42}$-evoked glutamate release differences among the DG, CA3, and CA1 supports the need to utilize *in vivo* recording techniques with high spatial resolution to be able to independently measure discrete subregions of larger anatomical CNS structures.

While our current studies support $A\beta_{42}$-evoked glutamate release is completely modulated through the α7nAChR, $A\beta_{42}$ can bind the α4β2nAChR at 100-5000 times higher concentration than α7nAChR [10]. Furthermore, Mura and colleagues [8] reported Aβ had a dual effect on the α7 and α4β2nAChR in the rat hippocampus. The biggest difference between these two studies was that Mura and colleagues conducted their experiments in awake, freely-behaving rats while our studies were performed in isoflurane anesthetized mice. Isoflurane has been shown to inhibit the α4β2, but not α7nAChR [37]. Based on these data, we cannot rule out a potential role for the α4β2 nAChR-$A\beta_{42}$ modulation of glutamate release.

Gahring and colleagues [38] have demonstrated that α7nAChR are located on both neurons and astrocytes, however the role of glial α7nAChR in glutamate release is unclear. For example, stimulation of astrocytic α7nAChR by nicotine has resulted in the release of glutamate from mouse cortical gliosomes [39], but Salamone and colleagues reported that perfusion of $A\beta_{40}$ onto rat hippocampal gliosomes inhibited glutamate overflow [40], which may result in decreased basal glutamate. Since the present studies support that $A\beta_{42}$ evokes glutamate release *in vivo*, we sought to determine the neuronal versus glial contribution by coapplying 0.1 μM $A\beta_{42}$ with 10.0 μM TTX. TTX is a reversible sodium channel blocker that prevents neuronal depolarization, while gliotransmission, the result of increased astrocytic intracellular calcium levels, would be unaffected. In the present study, coapplication of 0.1 μM $A\beta_{42}$ with 10.0 μM TTX completely blocked $A\beta_{42}$ mediated glutamate release and decreased basal glutamate levels as previously observed [27,41,42],

supporting Aβ$_{42}$-evoked glutamate release originating from predominantly neuronal activation of the α7nAChR. Furthermore, by blocking neuronal depolarization with TTX, the coapplied Aβ$_{42}$ could still bind astrocytic α7nAChR and synergistically depress basal glutamate. This may suggest a dual role for the α7nAChR whereby binding evokes neuronal glutamate release but blocks astrocytic glutamate release.

While excitotoxicity has been proposed as a mechanism of neuronal death and cognitive decline associated with AD [43], the concentration of Aβ$_{42}$-evoked glutamate release observed in this study is not in the neurotoxic range for an intact CNS abundant in glia under normal conditions [15]. Rather, the progressive accumulation of Aβ$_{42}$ during disease progression could lead to persistent activation of the α7nAChR and chronically elevate glutamate release that, over time, results in excitotoxicity. Soluble Aβ$_{42}$ levels have been shown to increase during AD progression in both humans [44,45] and mouse models of AD [34,46]. Furthermore, Aβ$_{42}$ causes protein oxidation of glutamine synthetase [47] and glutamate transporter 1 [48], the predominant isoform that accounts for ~90% of glutamate clearance from the extracellular space. As the soluble Aβ$_{42}$ concentration gradually increases, its neuromodulatory role on glutamate release is elevated while simultaneously decreasing glutamate clearance resulting in excitotoxicity, thereby initiating the cognitive decline associated with AD.

Furthermore, as the Aβ$_{42}$ concentration increases from a physiological neuromodulatory role to the pathological hallmark observed in AD, the α7nAChR-Aβ$_{42}$ interaction may advance AD etiology through several mechanisms. First, prolonged exposure to high nM concentrations of Aβ$_{42}$ has been shown to block or desensitize α7nAChR receptor function thereby preventing the normal function of these receptors [49]. Second, the α7nAChR-Aβ$_{42}$ complex may become internalized in both neurons and astrocytes, leading to plaque

formation and eventual host cell lysis and plaque deposition [50]. Third, the α7nAChR-Aβ$_{42}$ may serve as the initial scaffold for Aβ$_{42}$ aggregation and eventual plaque accumulation [10] resulting in AD neuropathological progression [36] as previously mentioned. Taken together, these data suggest that Aβ$_{42}$ accumulation causes a functional blockade of the α7nAChR that impairs neuromodulation and potentially cognition, which may support why drugs targeting the cholinergic and glutamatergic systems in later stages of AD are largely unsuccessful.

In conclusion, we have demonstrated that soluble, monomeric Aβ$_{42}$ can evoke glutamate release through the α7nAChR and release varies across hippocampal subfields. This release is mediated through a sodium channel dependent mechanism. Future studies will determine if dimeric and trimeric isoforms of Aβ$_{42}$-evoke or -inhibit glutamate release and determine the potential receptors through which these mechanisms occur.

References

[1]   Jack CR, Knopman DS, Jagust WJ, Petersen RC, Weiner MW, Aisen PS, Shaw LM, Vemuri P, Wiste HJ, Weigand SD, Lesnick TG, Pankratz VS, Donohue MC, Trojanowski JQ (2013) Tracking pathophysiological processes in Alzheimer's disease: an updated hypothetical model of dynamic biomarkers. *Lancet. Neurol.* **12**, 207–16.

[2]   Haass C, Selkoe DJ (2007) Soluble protein oligomers in neurodegeneration: lessons from the Alzheimer's amyloid beta-peptide. *Nat. Rev. Mol. Cell Biol.* **8**, 101–12.

[3]   Verdile G, Fuller S, Atwood CS, Laws SM, Gandy SE, Martins RN (2004) The role of beta amyloid in Alzheimer's disease: still a cause of everything or the only one who got caught? *Pharmacol. Res.* **50**, 397–409.

[4]   Jin M, Selkoe DJ (2015) Systematic analysis of time-dependent neural effects of soluble amyloid β oligomers in culture and in vivo: Prevention by scyllo-inositol. *Neurobiol. Dis.* **82**, 152–63.

[5]   Müller-Schiffmann A, Herring A, Abdel-Hafiz L, Chepkova AN, Schäble S, Wedel D, Horn AHC, Sticht H, de Souza Silva MA, Gottmann K, Sergeeva OA, Huston JP, Keyvani K, Korth C (2016) Amyloid-β dimers in the absence of plaque pathology impair learning and synaptic plasticity. *Brain* **139**, 509–25.

[6]   Shankar GM, Li S, Mehta TH, Garcia-Munoz A, Shepardson NE, Smith I, Brett FM, Farrell MA, Rowan MJ, Lemere CA, Regan CM, Walsh DM, Sabatini BL, Selkoe DJ (2008) Amyloid-beta protein dimers isolated directly from Alzheimer's brains impair synaptic plasticity and memory. *Nat. Med.* **14**, 837–42.

[7]   Mura E, Lanni C, Preda S, Pistoia F, Sarà M, Racchi M, Schettini G, Marchi M, Govoni S (2010) Beta-amyloid: a disease target or a synaptic regulator affecting age-related neurotransmitter changes? *Curr. Pharm. Des.* **16**, 672–83.

[8]   Mura E, Zappettini S, Preda S, Biundo F, Lanni C, Grilli M, Cavallero A, Olivero G, Salamone A, Govoni S, Marchi M (2012) Dual effect of beta-amyloid on α7 and α4β2 nicotinic receptors controlling the release of glutamate, aspartate and GABA in rat hippocampus. *PLoS One* **7**, e29661.

[9]   Varga E, Juhász G, Bozsó Z, Penke B, Fülöp L, Szegedi V (2014) Abeta(1-42) enhances neuronal excitability in the CA1 via NR2B subunit-containing NMDA receptors. *Neural Plast.* **2014**, 584314.

[10]   Wang H-Y, Lee DHS, Davis CB, Shank RP (2002) Amyloid Peptide Aβ1-42 Binds Selectively and with Picomolar Affinity to α7 Nicotinic Acetylcholine Receptors. *J. Neurochem.* **75**, 1155–1161.

[11]   Konradsson-Geuken A, Gash CR, Alexander K, Pomerleau F, Huettl P, Gerhardt GA, Bruno JP (2009) Second-by-second analysis of alpha 7 nicotine receptor regulation of glutamate release in the prefrontal cortex of awake rats. *Synapse* **63**, 1069–82.

[12]   Francis PT (2003) Glutamatergic systems in Alzheimer's disease. *Int. J. Geriatr. Psychiatry* **18**, S15–21.

[13]   Puzzo D, Privitera L, Leznik E, Fà M, Staniszewski A, Palmeri A, Arancio O (2008) Picomolar amyloid-beta positively

modulates synaptic plasticity and memory in hippocampus. *J. Neurosci.* **28**, 14537–45.

[14]   Zhou Y, Danbolt NC (2013) GABA and Glutamate Transporters in Brain. *Front. Endocrinol. (Lausanne).* **4**, 165.

[15]   Danbolt NC (2001) Glutamate uptake. *Prog. Neurobiol.* **65**, 1–105.

[16]   Hascup KN, Hascup ER (2015) Altered neurotransmission prior to cognitive decline in AβPP/PS1 mice, a model of Alzheimer's disease. *J. Alzheimers. Dis.* **44**, 771–6.

[17]   Hascup ER, af Bjerkén S, Hascup KN, Pomerleau F, Huettl P, Strömberg I, Gerhardt GA (2009) Histological studies of the effects of chronic implantation of ceramic-based microelectrode arrays and microdialysis probes in rat prefrontal cortex. *Brain Res.* **1291**, 12–20.

[18]   Nicholson C (2001) Diffusion and related transport mechanisms in brain tissue. *Reports Prog. Phys.* **64**, 815–884.

[19]   Hascup KN, Rutherford EC, Quintero JE, Day BK, Nickell JR, Pomerleau F, Huettl P, Burmeister JJ, Gerhardt GA (2006) Second-by-Second Measures of L-Glutamate and Other Neurotransmitters Using Enzyme-Based Microelectrode Arrays - Electrochemical Methods for Neuroscience - NCBI Bookshelf. In *Electrochemical Methods for Neuroscience*, Borland AC, Michael LM, eds. CRC Press, pp. 407–450.

[20]   Hascup KN, Hascup ER (2014) Electrochemical techniques for subsecond neurotransmitter detection in live rodents. *Comp. Med.* **64**, 249–55.

[21]   Burmeister JJ, Moxon K, Gerhardt GA (2000) Ceramic-based multisite microelectrodes for electrochemical recordings. *Anal. Chem.* **72**, 187–92.

[22]   Hinzman JM, Thomas TC, Burmeister JJ, Quintero JE, Huettl P, Pomerleau F, Gerhardt GA, Lifshitz J (2010) Diffuse brain injury elevates tonic glutamate levels and potassium-evoked glutamate release in discrete brain regions at two days post-injury: an enzyme-based microelectrode array study. *J. Neurotrauma* **27**, 889–99.

[23]   Hascup, K.N. Hascup, E.R., Littrell, O.M., Hinzmann J.M., Werner C.E., Davis V.A., Burmeister J.J., Pomerleau F., Quintero J.E., Huettl, P., Gerhardt GA (2013) Microelectrode Array Fabrication and Optimization for Selective Neurochemical Detection. In *Microelectrode Biosensors*, Marinesco S, Dale N, eds. Humana Press, Totowa, NJ, pp. 27–54.

[24]   Friedemann MN, Gerhardt GA (1992) Regional effects of aging on dopaminergic function in the Fischer-344 rat. *Neurobiol. Aging* **13**, 325–32.

[25]   Paxinos G, Franklin KBJ (2004) *The Mouse Brain in Stereotaxic Coordinates*, Gulf Professional Publishing.

[26]   Burmeister JJ, Gerhardt GA (2001) Self-referencing ceramic-based multisite microelectrodes for the detection and elimination of interferences from the measurement of L-glutamate and other analytes. *Anal. Chem.* **73**, 1037–42.

[27]   Hascup ER, Hascup KN, Stephens M, Pomerleau F, Huettl P, Gratton A, Gerhardt GA (2010) Rapid microelectrode measurements and the origin and regulation of extracellular glutamate in rat prefrontal cortex. *J. Neurochem.* **115**, 1608–1620.

[28]   Hascup KN, Hascup ER, Stephens ML, Glaser PEA, Yoshitake T, Mathé AA, Gerhardt GA, Kehr J (2011) Resting glutamate

levels and rapid glutamate transients in the prefrontal cortex of the Flinders Sensitive Line rat: a genetic rodent model of depression. *Neuropsychopharmacology* **36**, 1769–1777.

[29] Burmeister JJ, Pomerleau F, Palmer M, Day BK, Huettl P, Gerhardt GA (2002) Improved ceramic-based multisite microelectrode for rapid measurements of L-glutamate in the CNS. *J. Neurosci. Methods* **119**, 163–71.

[30] Magdesian MH, Nery AA, Martins AHB, Juliano MA, Juliano L, Ulrich H, Ferreira ST (2005) Peptide blockers of the inhibition of neuronal nicotinic acetylcholine receptors by amyloid beta. *J. Biol. Chem.* **280**, 31085–90.

[31] Khan GM, Tong M, Jhun M, Arora K, Nichols RA (2010) beta-Amyloid activates presynaptic alpha7 nicotinic acetylcholine receptors reconstituted into a model nerve cell system: involvement of lipid rafts. *Eur. J. Neurosci.* **31**, 788–96.

[32] Mehta TK, Dougherty JJ, Wu J, Choi CH, Khan GM, Nichols RA (2009) Defining pre-synaptic nicotinic receptors regulated by beta amyloid in mouse cortex and hippocampus with receptor null mutants. *J. Neurochem.* **109**, 1452–8.

[33] Parri HR, Hernandez CM, Dineley KT (2011) Research update: Alpha7 nicotinic acetylcholine receptor mechanisms in Alzheimer's disease. *Biochem. Pharmacol.* **82**, 931–42.

[34] Waters J (2010) The concentration of soluble extracellular amyloid-β protein in acute brain slices from CRND8 mice. *PLoS One* **5**, e15709.

[35] Tribollet E, Bertrand D, Marguerat A, Raggenbass M (2004) Comparative distribution of nicotinic receptor subtypes during development, adulthood and aging: an autoradiographic study in the rat brain. *Neuroscience* **124**, 405–20.

[36] Thal DR, Rüb U, Schultz C, Sassin I, Ghebremedhin E, Del Tredici K, Braak E, Braak H (2000) Sequence of Aβ-Protein Deposition in the Human Medial Temporal Lobe. *J. Neuropathol. Exp. Neurol.* **59**, 733–748.

[37] Flood P, Ramirez-Latorre J, Role L (1997) Alpha 4 beta 2 neuronal nicotinic acetylcholine receptors in the central nervous system are inhibited by isoflurane and propofol, but alpha 7-type nicotinic acetylcholine receptors are unaffected. *Anesthesiology* **86**, 859–65.

[38] Gahring LC, Persiyanov K, Dunn D, Weiss R, Meyer EL, Rogers SW (2004) Mouse strain-specific nicotinic acetylcholine receptor expression by inhibitory interneurons and astrocytes in the dorsal hippocampus. *J. Comp. Neurol.* **468**, 334–46.

[39] Patti L, Raiteri L, Grilli M, Zappettini S, Bonanno G, Marchi M (2007) Evidence that α7 nicotinic receptor modulates glutamate release from mouse neocortical gliosomes. *Neurochem. Int.* **51**, 1–7.

[40] Salamone A, Mura E, Zappettini S, Grilli M, Olivero G, Preda S, Govoni S, Marchi M (2014) Inhibitory effects of beta-amyloid on the nicotinic receptors which stimulate glutamate release in rat hippocampus: the glial contribution. *Eur. J. Pharmacol.* **723**, 314–21.

[41] Day BK, Pomerleau F, Burmeister JJ, Huettl P, Gerhardt GA (2006) Microelectrode array studies of basal and potassium-evoked release of L-glutamate in the anesthetized rat brain. *J. Neurochem.* **96**, 1626–35.

[42] Hascup KN, Hascup ER, Pomerleau F, Huettl P, Gerhardt GA (2008) Second-by-second measures of L-glutamate in the

prefrontal cortex and striatum of freely moving mice. *J. Pharmacol. Exp. Ther.* **324**, 725–731.

[43] Francis PT (2003) Glutamatergic systems in Alzheimer's disease. *Int. J. Geriatr. Psychiatry* **18**, S15–21.

[44] Wang J, Dickson DW, Trojanowski JQ, Lee VM (1999) The levels of soluble versus insoluble brain Abeta distinguish Alzheimer's disease from normal and pathologic aging. *Exp. Neurol.* **158**, 328–37.

[45] Lue LF, Kuo YM, Roher AE, Brachova L, Shen Y, Sue L, Beach T, Kurth JH, Rydel RE, Rogers J (1999) Soluble amyloid beta peptide concentration as a predictor of synaptic change in Alzheimer's disease. *Am. J. Pathol.* **155**, 853–62.

[46] Robert J, Stukas S, Button E, Cheng WH, Lee M, Fan J, Wilkinson A, Kulic I, Wright SD, Wellington CL (2015) Reconstituted high-density lipoproteins acutely reduce soluble brain Aβ levels in symptomatic APP/PS1 mice. *Biochim. Biophys. Acta* **1862**,1027-36.

[47] Boyd-Kimball D, Sultana R, Poon HF, Lynn BC, Casamenti F, Pepeu G, Klein JB, Butterfield DA (2005) Proteomic identification of proteins specifically oxidized by intracerebral injection of amyloid beta-peptide (1-42) into rat brain: implications for Alzheimer's disease. *Neuroscience* **132**, 313–24.

[48] Butterfield DA, Castegna A, Lauderback C, Drake J (2002) Evidence that amyloid beta-peptide-induced lipid peroxidation and its sequelae in Alzheimer's disease brain contribute to neuronal death1. *Neurobiol. Aging* **23**, 655–664.

[49] Liu Q, Kawai H, Berg DK (2001) beta -Amyloid peptide blocks the response of alpha 7-containing nicotinic receptors on hippocampal neurons. *Proc. Natl. Acad. Sci. U. S. A.* **98**, 4734–9.

[50] D'Andrea MR, Nagele RG, Wang H-Y, Peterson PA, Lee DHS (2001) Evidence that neurones accumulating amyloid can undergo lysis to form amyloid plaques in Alzheimer's disease. *Histopathology* **38**, 120–134.

Figure 1: *MEA and In Vitro Calibration*

A) Image of the R2 MEA used for anesthetized recordings with magnified tip (B) depicting 2 Pt recording sites measuring 50 x 100 μm with 100 μm spacing between sites. C) A typical MEA *in vitro* calibration measuring the change in current on a glutamate measuring site (green, top trace) and a sentinel recording site (blue, bottom trace) with the addition of multiple analytes (↓), as indicated. The addition of interferents such as AA and DA produced no current change on either site since they are blocked by the mPD exclusion layer. Three glutamate additions showed a stepwise increase of current on the glutamate oxidase / BSA / glutaraldehyde site, but no response on the BSA / glutaraldehyde sentinel site. The addition of H_2O_2 produced a similar increase of current on both recording sites. Finally, addition of $A\beta_{42}$ produced no change in current on either site indicating the peptide is not electrochemically active.

Figure 2: Hippocampal Basal Glutamate

Bar graph depicting basal glutamate in the DG (n=30), CA3 (n=31), and CA1 (n=29). Sample size refers to the number of animals in each hippocampal subfield. Basal glutamate measures were determined by taking a 10 s baseline average prior to local application of drug or saline control for each hippocampal subfield.

Figure 3: Local Application of $A\beta_{42}$

A)   Bar graph depicting a similar range of volumes was used for saline vehicle and all four concentrations for $A\beta_{42}$ *in vivo*. B) Representative trace of local application (↑) of $A\beta_{42}$-evoked glutamate release (top, black trace) versus saline control (bottom, gray) trace in the DG. C) Average glutamate response from local application of saline control and 0.01, 0.1, 1.0, 10.0 μM

Aβ$_{42}$. One-Way ANOVA with Fisher's LSD *post-hoc* *p<0.05, **p<0.01, ***p<0.001 versus saline control.

Figure 4: Coapplication of 0.1 µM Aβ$_{42}$ with 10.0 µM αBTx or 10.0 µM TTX

A) Bar graph depicting a similar range of volumes was used for 0.1 µM Aβ$_{42}$, 0.1 µM Aβ$_{42}$ with 10.0 µM αBTx, and 0.1 µM Aβ$_{42}$ with 10.0 µM TTX in all three hippocampal subfields studied. B) Representative trace of evoked glutamate release from local application (↑) of saline (second from bottom), 0.1 µM Aβ$_{42}$ (top), 0.1 µM Aβ$_{42}$ with 10.0 µM αBTx (second from top), and 0.1 µM Aβ$_{42}$ with 10.0 µM TTX (bottom) in the CA1. C) Average glutamate response from local application of 0.1 µM Aβ$_{42}$ with 10.0 µM αBTx was significantly attenuated versus 0.1 µM Aβ$_{42}$ in the DG, CA3, and CA1. Average glutamate response from local application of 0.1 µM Aβ$_{42}$ with 10.0 µM TTX blocked glutamate release that was significantly decreased versus 0.1 µM Aβ$_{42}$ in the DG, CA3, and CA1. Unpaired, two-tailed Student's t-test, *p<0.05, **p<0.01, ****p<0.0001 versus 0.1 µM Aβ$_{42}$.

Supplementary Figure 1: SDS-Page Gel

SDS-PAGE showing Coomassie G-250 stained proteins consistent with Aβ$_{42}$ monomer (4.5 kDA) in the 0.1, 1.0, and 10.0 µM evaluated *in vivo*. Once prepared, all solutions were maintained at room temperature for 60 minutes prior to gel loading; the same length of time the solution remains in the glass micropipette before local application studies are started.
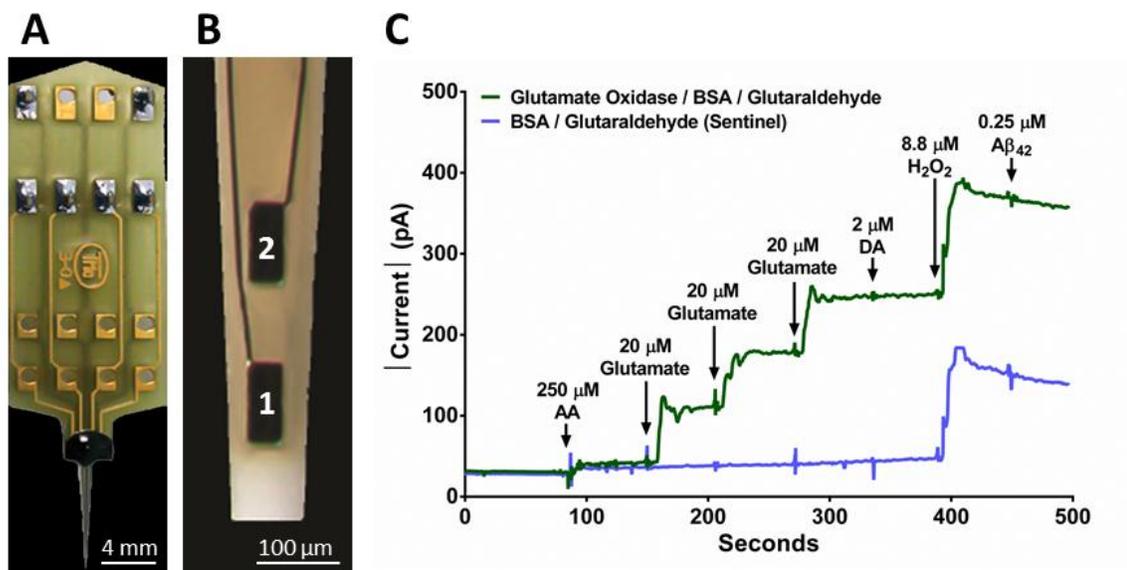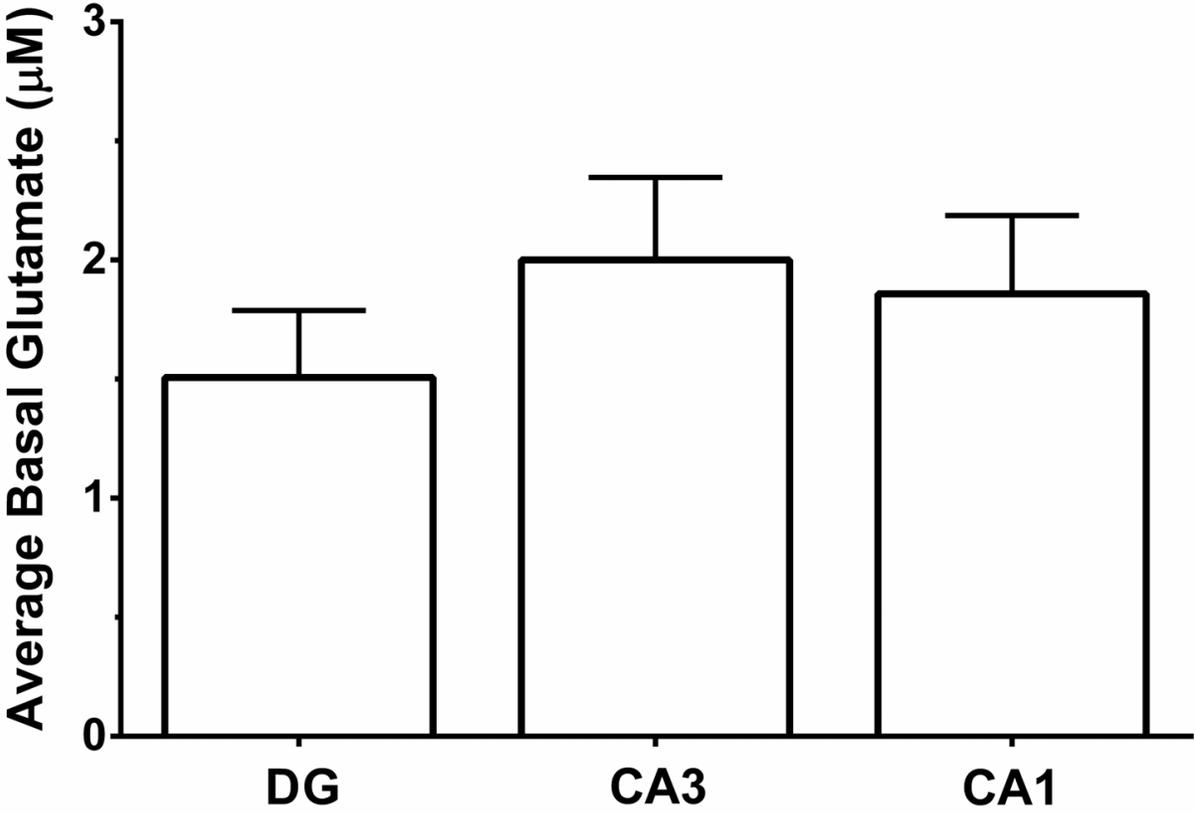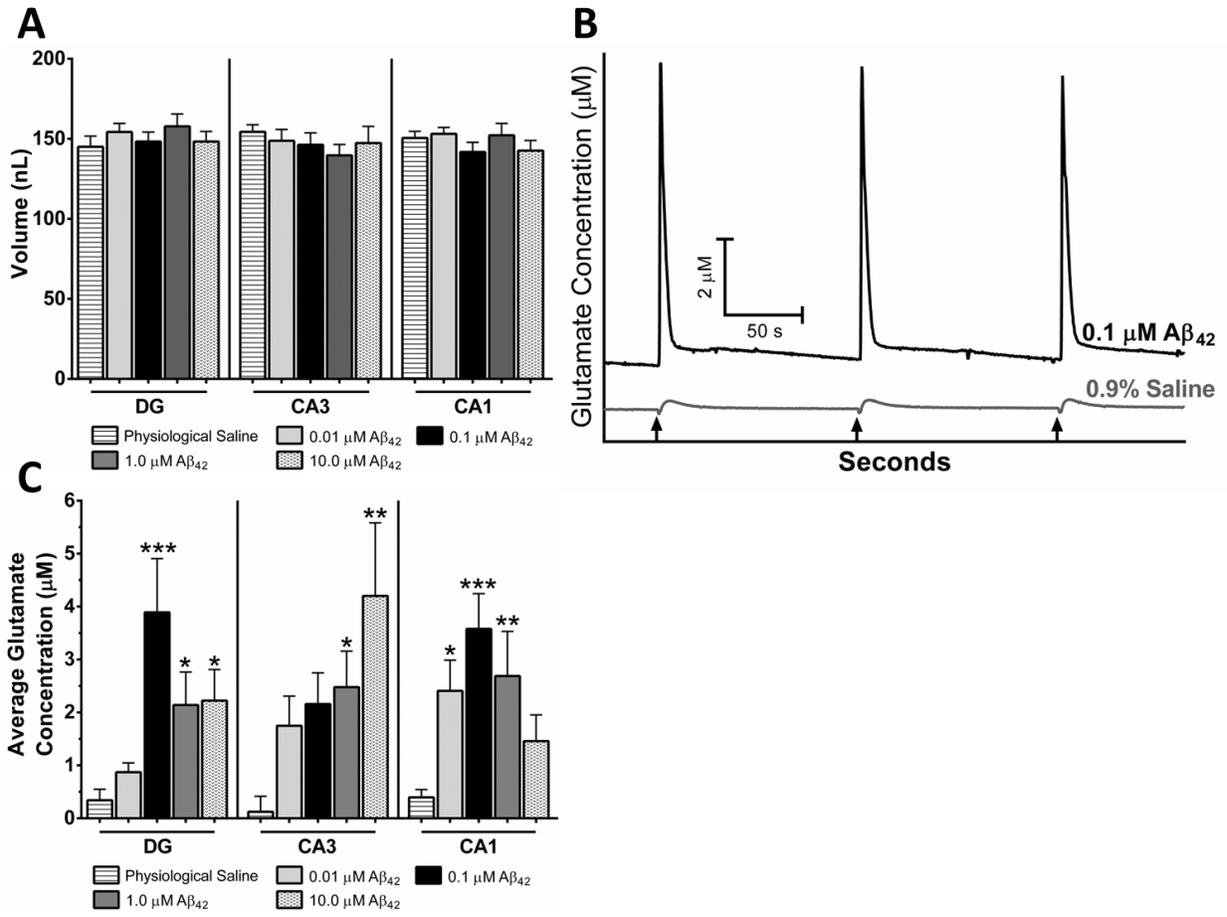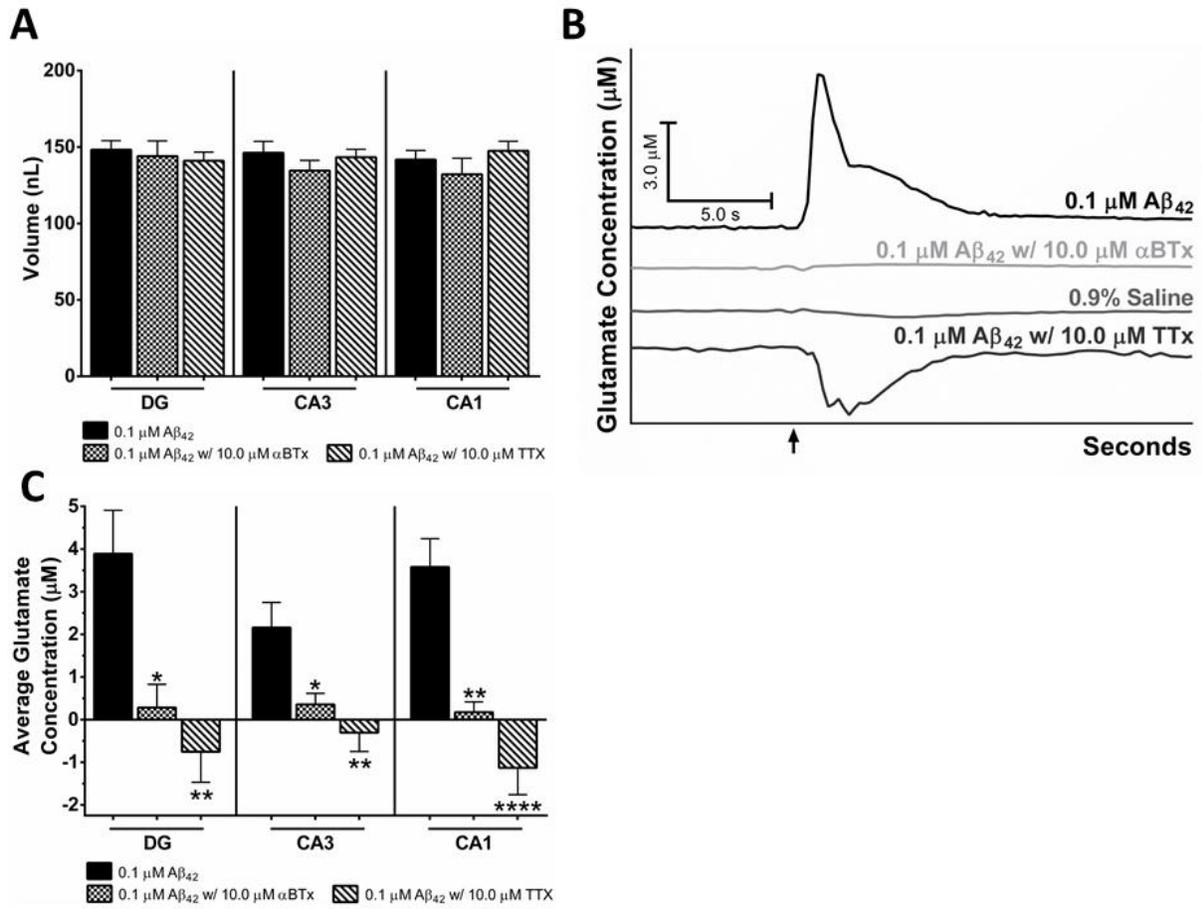
Figure 1

Figure 2

Figure 3

Figure 4

Supplemental Figure 1